Tuft cells transdifferentiate to neural-like progenitor cells in the progression of pancreatic cancer.

Daniel J. Salas-Escabillas[1,2]; Megan T. Hoffman, PhD[3]; Jacee S. Moore, MS[2]; Sydney M. Brender, MS[2]; Hui-Ju Wen, PhD[2]; Simone Benitz, PhD[2]; Erick T. Davis[2]; Dan Long[2]; Allison M. Wombwell[2]; Nina G. Steele, PhD[2]; Rosalie C. Sears, PhD[4]; Ichiro Matsumoto, PhD[5]; Kathleen E. DelGiorno, PhD[6]; Howard C. Crawford, PhD* [2, 7]

[1] Cancer Biology, University of Michigan, Ann Arbor, MI

[2] Department of Surgery, Henry Ford Health, Detroit, MI

[3] Department of Immunology, Dana-Farber Cancer Institute, Harvard Medical School, Boston, MA

[4] Department of Molecular and Medical Genetics, Oregon Health & Science University, Portland, OR

[5]Monell Chemical Senses Center, Philadelphia, PA

[6]Department of Cell and Developmental Biology, Vanderbilt University School of Medicine, Nashville, TN

[7] Cancer Biology Program, Wayne State University, Detroit, MI

*Corresponding Author:

Howard C. Crawford, PhD, Department of Surgery, Henry Ford Health System, Detroit, Michigan, USA

Email: hcrawfo1@hfhs.org

Summary

Pancreatic ductal adenocarcinoma (PDA) is partly initiated through the transdifferentiation of acinar cells to metaplastic ducts that act as precursors of neoplasia and cancer. Tuft cells are solitary chemosensory cells not found in the normal pancreas but arise in metaplasia and neoplasia, diminishing as neoplastic lesions progress to carcinoma. Metaplastic tuft cells (mTCs) function to suppress tumor progression through communication with the tumor microenvironment, but their fate during progression is unknown. To determine the fate of mTCs during PDA progression, we have created a lineage tracing model that uses a tamoxifen-inducible tuft-cell specific Pou2f3$^{CreERT/+}$ driver to induce transgene expression, including the lineage tracer tdTomato or the oncogene *Myc*. mTC lineage trace models of pancreatic neoplasia and carcinoma were used to follow mTC fate. We found that mTCs, in the carcinoma model, transdifferentiate into neural-like progenitor cells (NRPs), a cell type associated with poor survival in PDA patients. Using conditional knock-out and overexpression systems, we found that *Myc* activity in mTCs is necessary and sufficient to induce this Tuft-to-Neuroendocrine-Transition (TNT).

36 **Introduction**

37 Pancreatic ductal adenocarcinoma (PDA), the most common form of pancreatic
38 cancer, is a devastating disease with a 5-year survival rate of only 13% [1]. Effective treatment
39 options are few, and reliable early detection methods needed to enhance treatment
40 effectiveness are non-existent. PDA is initiated by oncogenic mutations in the *KRAS* gene,
41 causing irreversible transdifferentiation of normal acinar cells into metaplastic ducts.
42 Metaplastic ducts then progress to pancreatic intraepithelial neoplasia (PanIN) [2] and, with the
43 acquisition of mutations in tumor suppressor genes such as *TP53*, *CDKN2A*, or *SMAD4* [3, 4],
44 progress to invasive carcinoma. Metaplastic ducts are a heterogeneous population of
45 reactive epithelial cells [5] comprised of at least 6 distinct identities: gastric neck cells [6], gastric
46 pit-like cells, gastric chief-like cells, ductal senescent cells, metaplastic neuroendocrine cells
47 (mNECs), and specialized chemosensory cells known as metaplastic tuft cells (mTCs) [7].

48 Normal tuft cells are solitary chemosensory cells found throughout the body that sense
49 and respond to environmental cues to maintain tissue homeostasis. Functionally, they use
50 the canonical gustatory signal transduction pathway, with specific stimulants and responses
51 depending on context and the organ in which they reside [8-10]. In pancreatic neoplasia,
52 metaplastic tuft cells (hereafter referred to as mTCs) have been proposed to be a class of
53 tumor progenitor cells [9, 11]. Still, functionally, they suppress progression to PDA via inhibition
54 of anti-inflammatory immune cells through crosstalk with the tumor microenvironment [8, 10].
55 mTCs are identified by staining for markers such as Acetylated-*Tuba1a*[10], *Dclk1*, *Vav1*,
56 *Cox1*[9], *Cox2*[12-14], *Trpm5* [15], and *Pou2f3*, the latter being the master transcriptional regulator
57 of tuft cell genesis [15, 16]. mTCs are not typically found in the normal pancreas and only
58 appear after prolonged damage, such as in chronic pancreatitis [17] or the initiation of
59 neoplasia [9, 11], arising from the transdifferentiation of acinar cells. As neoplasia progresses to

60 invasive carcinoma, the mTC population gradually disappears [9, 11], challenging their putative
61 role as classic tumor progenitor cells.

62 In the current study, to address the hypothesis that mTCs act as tumor progenitor cells
63 in pancreatic cancer, we lineage-traced their fate during disease progression in mouse
64 models of pancreatic disease. To accomplish this, we used a dual recombinase model
65 wherein tumorigenesis is initiated by the expression of FlpO recombinase knocked into the
66 pancreas-specific *Ptf1a* locus, driving the expression of an Frt-STOP-Frt oncogenic *Kras*$^{G12D/+}$
67 allele and the deletion an Frt-flanked allele of *Trp53* [18]. This model allowed us to use an
68 inducible *Pou2f3*$^{CreERT/+}$ driver [19] to target the expression of a *ROSA26*$^{LSL\text{-}TdTomato}$ lineage
69 trace reporter specifically to mTCs [16, 20] in both neoplasia and carcinoma, indelibly labeling
70 mTCs and their progeny. In the *Ptf1a*$^{FlpO/+}$*; Kras*^{G12D} neoplasia model, mTCs and other
71 metaplastic cellular subtypes, including neuroendocrine-like enteroendocrine cells [7, 21, 22]
72 arise from acinar cells, independent from one another. However, in the *Ptf1a*$^{FlpO/+}$*; Kras*$^{FSF\text{-}G12D/+}$*; Trp53*$^{Frt\text{-}Exons\ 2\ to\ 5\text{-}Frt/+}$ carcinoma model, we found that acinar cell-derived mTCs
74 transdifferentiate to neural-like progenitor cells (NRPs) [21], also known as ductal
75 neuroendocrine cells [23]. NRPs in PDA patients correlate with worse survival, are resistant to
76 chemotherapy, and their genesis is associated with elevated *MYC* activity [21, 23]. Indeed,
77 modulating the expression of *Myc* to mTCs demonstrated that *Myc* activity was necessary
78 and sufficient to drive the transdifferentiation of mTCs to NRPs.

RESULTS

Pou2f3-CreERT specifically targets recombination in metaplastic tuft cells in the pancreas.

Tuft cells are not found in the normal mouse pancreas but arise from the transdifferentiation of acinar cells in conditions of tissue damage and early neoplasia [24]. As neoplasia progresses, metaplastic tuft cells (mTCs) decrease in number and are absent in carcinoma [9, 11, 24]. To determine the fate of mTCs during neoplastic progression, we developed a novel dual recombinase lineage trace system, wherein Ptf1a$^{Flpo/+}$ [25] initiates expression of oncogenic Kras from a Kras$^{Frt\text{-}Stop\text{-}Frt\text{-}G12D}$ allele (*KF*) to drive neoplasia [18] (Fig. 1A, 1D). When combined with a conditional knock-out trp53 allele with exons 2-5 flanked by Frt recombination sites (Trp53$^{Frt\text{-}Exons\ 2\ to\ 5\text{-}Frt/+}$), lesions rapidly progress from neoplasia to carcinoma (*KPF*) (Fig. 1B, 1D). Within this system, we introduced a Cre^{ERT} driver knocked into the *Pou2f3* locus [19], which encodes the transcription factor master regulator of tuft cell genesis [15, 16, 20, 26, 27]. *Pou2f3$^{CreERT/+}$* was used to drive recombination and expression of a *ROSA26$^{LSL\text{-}tdTomato}$* reporter (tdTom) [28] in a tamoxifen-inducible manner (P2f3T) [8, 20, 27], allowing us to lineage trace mTCs temporally in our neoplasia (*KF-P2f3T)* and carcinoma (*KPF-P2f3T)* models.

To determine the fidelity of our systems in labeling tuft cells, we treated *KF-P2f3T* with cerulein at 8-9 weeks of age to induce mild pancreatitis and accelerate transformation, then allowed the mice to recover for 3 weeks to optimize mTC genesis [9, 11]. The *KPF-P2f3T* carcinoma model induced sufficient transformation and mTC formation at 11-12 weeks of age with no additional treatment (Fig. 1C). Cerulein-treated *KF-P2f3T* and 11–12-week-old *KPF-P2f3T* mice were treated with tamoxifen to induce tdTom reporter activity, and the pancreata

102 harvested 1 day later. We co-stained tissues for tdTom and the tuft cell markers Pou2f3,
103 Acetylated-α-tubulin, Cox1, Dclk1, Trpm5, and Vav1 (Fig. 1E and Supp. Fig. 1A, 1B) by
104 immunofluorescence (IF). In both models, we found co-expression of tdTom exclusively in
105 cells expressing mTC markers (Supp. Fig. 1A, 1B), confirming the system's specificity and
106 allowing us to trace mTC fate throughout the progression of PDA.

107 **Metaplastic tuft cells change identity in pancreatic adenocarcinoma.**

108 To determine the fate of the mTC population over time, we collected tissue from our
109 *KF-P2f3T* and *KPF-P2f3T* mice 3 days and 7 weeks post-tamoxifen. In the *KF-P2f3T*
110 neoplasia model, all tdTom$^+$ cells co-expressed tuft cell markers (Fig. 2A). The population of
111 mTCs dropped off slightly over this period but largely remained stable (Fig. 2B, *Black*). In
112 contrast, in the *KPF-P2f3T* carcinoma model, the mTC population dropped drastically by 7
113 weeks, consistent with their disappearance as PanIN progresses to PDA [9, 11] (Fig. 2A and 2B,
114 *Black*). We found no evidence that mTC attrition was associated with apoptosis by co-
115 staining for cleaved caspase 3 (CC3) (Fig. 1F). Instead, we noted that tdTom$^+$ cells persisted
116 in this model but no longer expressed mTC markers (Fig. 2A), suggesting that mTCs take on
117 a new cellular identity.

118 Quantitation of the tdTom expression throughout multiple pancreata revealed that, in
119 the *KPF-P2f3T* carcinoma model, the Cox1$^+$ mTC population dropped from an average of
120 15% at 3 days post-tamoxifen to an average of 3% at 7 weeks post-tamoxifen (Fig. 2B,
121 *Black*). In contrast, the mTC progeny population, defined as tdTom$^+$ cells not expressing
122 Cox1, increased by ~5-fold from an average of 4% of pancreatic ducts at 3 days post-
123 tamoxifen to an average of nearly 17% at 7 weeks post-tamoxifen, reflecting the degree of
124 mTC loss (Fig. 2B, *Pink*). These data support mTCs adopting a new identity in carcinomas.

125 **Transdifferentiation of mTCs to metaplastic neuroendocrine cells.**

126 To investigate the identity of the mTC progeny, we co-stained for tdTom together with
127 markers of the known identities of other metaplastic ductal cells defined by *Schlesinger et al*.
128 and *Benitz et al.*, including gastric pit-like (Gkn1$^+$), gastric neck-like (Lectin GS-II$^+$) [29], and
129 metaplastic neuroendocrine cells (Syp$^+$) [7, 9, 17].

130 The lack of co-expression of tdTom with Gkn1 or Lectin GS-II suggested that *KPF-*
131 *P2f3T* tdTom$^+$ mTC progeny had not taken on gastric pit-like cell or gastric neck-like cell
132 identities (Fig. 2C and Supp. Fig. 2A). Instead, mTC progeny stained positive for Syp,
133 revealing the acquisition of a metaplastic neuroendocrine cell (mNEC) identity (Fig. 2C,
134 *Yellow arrows*). To determine if tdTom expression in cells with a neuroendocrine phenotype
135 could be due to previously unnoticed recombination in pancreatic islets, we confirmed no co-
136 localization of tdTom co-staining with Insulin (Ins) or in surrounding islet cells (Supp. Fig. 2B).
137 Quantitation of the different time points for the *KPF-P2f3T* model confirmed a decrease of
138 tdTom$^+$/Cox1$^+$ mTCs, (Fig. 2E, *Black*), with a concomitant ~4-fold increase of tdTom$^+$/Syp$^+$
139 mNECs, (Fig. 2E, *Pink*) by 7 weeks post-tamoxifen (Fig. 2D, 2E). Interestingly, while there is
140 a mNEC population in the metaplastic ducts in the *KF-P2f3T* neoplasia model, none
141 expressed tdTom, suggesting that they did not derive from mTCs (Fig. 2D, 2E, *Green*) and
142 had a distinct origin from those in the *KPF-P2f3T* mice.

143

144 **mNECs depend on the mTC population to develop in PDA but not PanIN models.**

145 Lineage tracing experiments show that mNECs in both neoplasia and carcinoma
146 models are initially derived from acinar cells [9] (Supp. Fig 2C) but differ in that carcinoma
147 mNECs derive from an mTC intermediate. As an independent test of these divergent origins,
148 we took advantage of our *Pou2f3*$^{CreERT/+}$ driver being a knock-in to the *Pou2f3* allele, thus
149 inactivating endogenous Pou2f3 activity [20]. By creating a model homozygous for
150 *Pou2f3*$^{CreERT/CreERT}$, we effectively ablated *Pou2f3* (Supp. Fig. 3A, 3B), preventing mTC
151 formation [8] and, therefore, any mTC progeny. Consistent with our previous observations,
152 Cox1^{+} mTC and Syp^{+} mNEC populations were easily identifiable in the pancreatic lesions of
153 our KF; Pou2f3$^{CreERT/+}$ neoplasia model. Pou2f3 ablation in these mice eliminated the mTC
154 population, as expected, while the mNEC population persisted (Fig. 3A), supporting their
155 independent origins. In contrast, in the KPF; Pou2f3$^{CreERT/CreERT}$ carcinoma mice, we found
156 neither mTCs nor mNECs, confirming a shared dependency on Pou2f3 function (Fig. 3A,
157 *Green arrows*).

158 Lineage tracing and Pou2f3 ablation data in KPF mice support a model where mTCs
159 give rise to mNECs. However, it was also possible that in the KPF model, both cell types
160 express *Pou2f3* and require its activity. mNECs do not express *Pou2f3* in *Kras*^{G12D}-driven
161 neoplasia [7, 22, 27] but have not been examined in the KPF carcinoma model. To address this,
162 we performed co-immunofluorescence for Pou2f3, together with Cox1 (mTCs) and Syp
163 (mNECs). As expected, Pou2f3 was readily detectable in mTCs in both KF and KPF
164 pancreata (Fig 1E, 3B). In contrast, we found no examples of Pou2f3^{+} mNECs in either
165 system (Fig. 3B). The lack of identifiable recombination in early mNECs suggests that the
166 increasing population of tdTom^{+} mNEC cells is dependent on the prior genesis of the mTC
167 population.

168 **mTCs transdifferentiate into mNECs in PDA.**

169 The observation that mTCs act as a precursor cell to mNECs suggested two possible
170 models for this relationship: mTCs act as a stem-like cell, giving rise to mNEC daughter cells,
171 or alternatively, they directly transdifferentiate to mNECs. To distinguish these possibilities,
172 we tested if mNEC genesis had undergone DNA replication, consistent with them arising from
173 an asymmetric cell division of mTCs. mTCs rarely proliferate in neoplasia models [30], but their
174 proliferative capacity has not been examined in a carcinoma model.

175 Initially, we co-stained for Ki67 and Syp and found that, like mTCs, mNECs were not in
176 the cell cycle in *KF-P2f3T* or *KPF-P2f3T* mice (Fig. 3C, *Black arrows*). To test if a rare cell
177 division event was necessary for mNEC genesis, we used a long-term EdU incorporation
178 assay to determine if mNECs had gone through a prior cell division [9, 11]. *KPF-P2f3T* mice
179 were treated with tamoxifen once daily for 5 days at 11-12 weeks of age. We treated mice
180 with EdU every 12 hours for 3 days and collected pancreata 12 hours after the last injection.
181 Although we identified several EdU+ cells in the tissue (*Magenta arrows)*, neither Cox1^{+}
182 mTCs (*Green arrows)* nor Syp^{+} TNTs (*White arrows*) had incorporated EdU (Fig. 3D), and,
183 given the relatively long-time frame to allow for incorporation, were unlikely to have
184 proliferated prior to their appearance.

185 To test the alternative that mTC-derived mNECs arise from the direct
186 transdifferentiation of mTCs, we hypothesized that there would be cells that exist in mid-
187 transition, co-expressing markers of both mTCs (Cox1) and mNECs (Syp). To identify
188 transitionary cells, we co-stained Cox1 and Syp in *KPF-P2f3T* mice at 7 weeks post-
189 tamoxifen treatment. Although rare, we identified cells expressing both Cox1 and Syp (Fig.
190 3E, *Yellow arrows*) exclusively in *KPF-P2f3T* mice. These transitionary cells were also EdU

191 negative (Supp. Fig. 3C, *Yellow arrows*). Collectively, our data support a "Tuft-to-
192 Neuroendocrine Transition" (TNT) transdifferentiation event, analogous to an epithelial-to-
193 mesenchymal transition, exclusively in our pancreatic carcinoma model.

194 **Neoplastic mNECs have an enteroendocrine phenotype.**

195 While we have found mNECs in the pancreata of both neoplasia and carcinoma
196 models, they appear to have distinct cellular origins. We confirmed that mNECs and mTCs in
197 both models derive from acinar cells [17, 22] using an acinar cell lineage trace of *Pt1fa*$^{Cre/+}$;
198 *ROSA26*$^{LSL\text{-}YFP/+}$ in neoplasia and carcinoma models. We show co-localization with GFP (to
199 mark acinar cells and progeny) and either Cox1 (mTCs) or Syp (mNECs) for both models
200 (Supp. Fig. 2C). Although mNECs derive from acinar cells in neoplasia and carcinoma, in the
201 *KPF-P2f3T* carcinoma model, mNECs require the genesis of an mTC intermediate. This
202 unexpected observation led us to ask if mNECs in the *KF-P2f3T* neoplasia model and the
203 *KPF-P2f3T* carcinoma model are distinct identities.

204 Two types of mNECs are described in human pancreatic disease: neuroendocrine-like
205 cells [21], also designated enteroendocrine cells (EECs) [17, 22], marked by their expression of
206 islet cell hormones, and neural-like progenitor cells (NRPs) [21], also called ductal
207 neuroendocrine cells [7, 23], marked by the expression of genes associated with neural
208 development. EECs are distinct from tuft cells in their origins in pancreatic disease [17, 22] in
209 that they do not rely on Pou2f3 activity [17, 22, 31], and express markers of normal islet cells [21, 22].
210 To determine if mNECs in our models bore an EEC phenotype, we examined islet cell
211 hormone expression [21] by co-IF of wide-spectrum cytokeratin (PanCK) and Syp together with
212 either glucagon (Gcg), insulin (Ins), somatostatin (Sst), pancreatic polypeptide (Ppy), and
213 ghrelin (Ghrl), markers of α, β, δ, γ, and ε islet cells, respectively [32].

214 Since the KF mNECs do not express a lineage tracer, we confined our analysis to
215 PanCK$^+$/Syp$^+$ cells to distinguish them from singular islet cells that can become trapped
216 within the diseased tissue (Figs. 4A-E & Supp. Fig. 3D). In the *KF-P2f3T* neoplasia model,
217 we consistently found isolated mTC-independent mNECs expressing islet cell identity
218 markers apart from the β cell markers Ins and serotonin (5-HT) (Fig. 4B and Supp. Fig. 2B).
219 In contrast, we found no islet hormone expression in the mTC-derived mNECs in the *KPF-*
220 *P2f3T* mouse. These data indicated that mNECs in our KF-P2f3T neoplasia model, but not in
221 our *KPF-P2f3T* carcinoma model, are likely EECs, similar to those found in other models of
222 pancreatic disease [17, 21, 22].

223 **Cells derived from TNT persist in pancreatic carcinoma.**

224 Having established that mNECs in KF neoplasia are likely EECs, whereas those in the
225 KPF carcinoma are not, we hypothesized that the TNT-derived mNECs are neural-like
226 progenitor cells (NRPs), as identified in human PDA [21]. In human PDA, NRPs correlate with
227 poor survival and drug resistance [23]. Initially, we asked if our TNT mNECs persist in frank
228 carcinoma, as NRPs do in patients. To test this, we extended the trace time post-tamoxifen
229 treatment to 12 weeks and examined tdTom expression in areas of undifferentiated
230 carcinoma, confirmed by histology (data not shown). As expected, tuft cells were absent in
231 regions of carcinoma, as indicated by IHC for Dclk1 (Fig. 5A, *Left*). However, when we
232 stained adjacent sections for tdTom, we easily found mTC progeny cells scattered throughout
233 the tumors (Fig. 5A, *Right*). Using co-IF, we confirmed that the identity of these mTC
234 progeny were indeed Syp-expressing mNECs (Fig. 5B). We conclude that not only are mTCs
235 undergoing TNT, but the mTC-derived mNECs persist within dedifferentiated carcinoma,
236 consistent with NRPs in PDA patients [21].

237 **TNT gives rise to Nrxn3^{+} neural-like progenitor cells in pancreatic carcinoma.**

238 Neurexin 3 (Nrxn3) is a marker of neural-like progenitor cells (NRPs) linked with poor
239 prognosis and chemotherapy resistance in multiple cancers, including colon, lung, and
240 pancreatic cancer [21, 33, 34]. The persistence of mNECs in carcinoma led us to examine the
241 expression of Nrxn3 in the TNT-derived mNECs in the KPF carcinoma model. KF neoplasia
242 and KPF carcinoma tissues were co-stained for Nrxn3, Syp, and PanCK to distinguish
243 mNECs with an NRP identity. As expected, *KF-P2f3T* EECs did not express Nrxn3 (Fig. 6A
244 and 6B, *Top*). However, in the *KPF-P2f3T* carcinoma model, Nrxn3, Syp, and PanCK co-
245 localization confirmed that TNT-derived mNECs cells were indeed NRPs both in areas of
246 neoplasia (Fig. 6A and 6B, *Bottom*) and carcinoma (Fig. 6C).

247 **The Tuft to Neuroendocrine transition is dependent upon *Myc* activity.**

248 Pancreatic parenchyma-wide *Myc* activity induces the formation of mNECs in a KC
249 model of neoplasia [23], similar to the prostate and lung [35-38]. NRPs in patient samples are
250 marked by high levels of MYC activity in cancers of the pancreas and other tissues [21, 23, 35, 36].
251 We hypothesized that targeting *Myc* activity specifically to mTCs in the *KF-P2f3T* neoplasia
252 mouse, where TNT is not otherwise observed, would be sufficient to induce NRP genesis. To
253 accomplish this, we crossed the *Myc* Cre-dependent overexpression mouse line, ROSA26^{LSL-}
254 $^{cMyc/+}$, into the *KF-P2f3T* model (designated KF-MOE) (Supp. Fig. 4A). We treated these mice
255 with cerulein to induce transformation and mTC genesis, then treated with tamoxifen 3 weeks
256 later to activate the tdTom reporter and induce upregulation of *Myc* specifically in the mTCs.
257 As previously observed, the control *KF-P2f3T* mice had no mTC-derived mNECs. In
258 contrast, we readily found mTC-derived mNEC genesis in KF-MOE tissue as early as 3 days
259 post-induction (Fig. 7A and Supp. Fig. 4C), *Yellow arrows*), with a 6-fold increase in the

260 tdTom^{+} mNEC population 7 weeks post-tamoxifen treatment (Fig 7C, *Pink*). Finally, to
261 determine if the mNECs in the *KF-MOE* mice were NRPs, we co-stained tissue 7 weeks post-
262 tamoxifen for Nrxn3, Syp, and tdTom (Fig. 7B). Indeed, we consistently found NRP identity in
263 the neuroendocrine population induced by overexpressing *Myc* in mTCs. Thus, *Myc*
264 expression targeted to mTCs is sufficient to induce transdifferentiation to NRPs in a neoplasia
265 model where NRPs are not observed otherwise.

266 Having shown that Myc activity is sufficient to drive TNT, we tested if it was necessary
267 for the process. To accomplish this, we crossed a conditional *Myc* knock-out allele (*Myc*$^{fl/+}$)
268 into the *KPF-P2f3T* model (designated *KPF-P2M*$^{fl/+}$) (Supp. Fig. 4B). These mice were
269 treated with tamoxifen to simultaneously activate the tdTom reporter and reduce *Myc* activity
270 specifically in the mTCs. As previously, the *KPF-P2f3T* control at 7 weeks post-tamoxifen
271 showed a lack of mTCs and an increased population of mTC-derived mNECs (Fig. 7D). In
272 contrast, in the *KPF-P2M*$^{fl/+}$ pancreata, we could easily identify Cox1^{+}/tdTom^{+} mTCs at 7
273 weeks post-tamoxifen (Fig. 7D&E) and a lack of Syp^{+}/tdTom^{+} mTC-derived mNECs.
274 Unexpectedly, these mice had a significant population of Syp^{+}/tdTom^{-} mTC-independent
275 mNECs (Fig. 7D; Supp. Fig 4D). To test if the mTC-independent mNECs were EECs, we
276 combined antibodies for Ghrl, Gcg, Sst, Ppy, and Ins to identify any hormone-positive cells
277 simultaneously and co-stained for tdTom (Fig. 7E). Indeed, the tdTom^{-} mNECs in the *KPF-*
278 *P2M*$^{fl/+}$ model expressed islet hormones, confirming their identity as EECs. We conclude that
279 *Myc* activity is necessary and sufficient to induce mTC transdifferentiation into NRPs.

280 **Discussion**

281 In the pancreas, prolonged injury or expression of oncogenic *Kras* leads to acinar-to-
282 ductal metaplasia, with metaplastic ducts comprised of at least 6 different cell types: gastric

283 pit-like cells, gastric chief-like cells, gastric SPEM/neck-like cells [6], senescent duct cells,
284 metaplastic neuroendocrine cells (mNECs), and metaplastic tuft cells (mTCs) [7, 9, 17]. The
285 functions of these different metaplastic cell types have only begun to be recognized. For
286 instance, normal tuft cells in other organs combat infection [14] and promote wound healing [11,
287 30, 39]. Consistent with their overall role in maintaining normal tissue homeostasis, mTCs
288 suppress the progression of pancreatic neoplasia to adenocarcinoma [8, 10]. In contrast,
289 mNECs in the pancreas are associated with tumor cell-neuron cross talk and promote tumor
290 cell proliferation [40].

291 While mTCs functionally hinder the progression of neoplasia to pancreatic cancer, they
292 also have been theorized to be tumor progenitor cells in the pancreas[11, 30, 41], intestine [42], and
293 stomach [43]. Doublecortin-like kinase (Dclk1), a common tuft cell marker, is also a marker of
294 progenitor cells in the pancreas and intestine [11, 30, 42]. Dclk1 is a microtubule kinase highly
295 expressed in neurons and is linked with neuronal survival and migration in other organs [44].
296 Besides Dclk1, mTCs express other stem cell markers such as CD133, CD24, and CD44 [11],
297 which, together with their low proliferation rate [11, 30, 42, 45], support their role as putative cancer
298 stem cells. Consistent with a facultative progenitor cell function, depleting mTCs delays
299 tissue repair after experimental pancreatitis [30, 42]. However, contrary to their proposed role as
300 cancer-initiating cells in PDA, mTC numbers diminish as neoplasia progresses to carcinoma
301 [9, 11], inconsistent with their mandatory role in the genesis of new tumors.

302 We theorized many possible reasons why mTCs disappear through progression. With
303 little evidence that they are dying or being outcompeted by more proliferative cell types, we
304 focused on the possibility that they were changing their cellular identity. Using a unique dual
305 recombinase mouse model to trace mTC fate through progression, we found that mTCs were
306 stable in *Kras*^{G12D}-driven neoplasia but transdifferentiated to a mNEC identity in a *Kras*^{G12D};

307 *Tp53*$^{+/-}$ carcinoma model. Importantly, we cannot distinguish whether it is progression to a
308 less differentiated adenocarcinoma in general or the deletion of a *Tp53* allele specifically that
309 is responsible for driving this transition. However, given that we do not observe mTCs or
310 their progeny in carcinomas derived from *Kras*^{G12D} expression only (data not shown), this
311 suggests an association with general tumor progression, agnostic to specific tumor
312 suppressor gene mutations.

313 Pancreatic tumor cells expressing neural/neuroendocrine markers in human PDA and
314 are comprised of two different subsets: neuroendocrine-like or enteroendocrine cells (EECs)
315 [7, 22] and neural-like progenitor cells (NRPs) [21], the latter of which is associated with poor
316 outcomes. EECs express hormone markers typically confined to islet cells [17, 21, 22], whereas
317 NRPs express markers of neural progenitor cells, including Nrxn3 [21]. We found that mNECs
318 in *Kras*^{G12D}-driven neoplasia arise independent of mTCs and take on an islet hormone-
319 positive EEC identity, consistent with previous data showing EECs in metaplasia are
320 independent of mTCs and do not depend on *Pou2f3* to develop [22]. In contrast, mNECs in
321 *Kras*^{G12D}*; Trp53*$^{+/-}$ carcinoma do derive from mTCs and have an Nrxn3^{+} NRP phenotype.
322 EECs share a seemingly similar fate as mTCs in that they are present at early stages of ADM
323 but diminish as PDA progresses to dedifferentiated carcinoma [22]. Our data support an
324 association of EECs with early oncogenesis as they are largely confined to our neoplasia
325 model and absent in our carcinoma model. Unexpectedly, ablation of a single allele of *Myc* in
326 the carcinoma model mTCs allowed EECs to reemerge, suggesting an inverse relationship
327 between EECs and NRPs.

328 Mouse mNECs (both EECs and NRPs) derive from acinar cells [17, 22, 23], but NRPs
329 require an mTC intermediate. NRPs are associated with high *Myc* activity in PDA and other
330 carcinomas such as lung, colon, and prostate cancer [21, 23, 35, 36]. Supporting the orthologous

331 nature of mouse NRP cells, upregulating *Myc* expression specifically in mTCs in our
332 neoplasia model was indeed sufficient to drive NRP transdifferentiation whereas reducing
333 *Myc* activity in the mTCs of our carcinoma model inhibited the process. Together, these data
334 suggest that *Myc* is both necessary and sufficient for a "tuft to neural progenitor transition"
335 (TNT) in PDA. NRPs contribute to tumorigenicity [46] and advanced carcinomas frequently
336 express neural characteristics [47], consistent with their association with poor outcomes in PDA
337 patients [21, 23] and our observation that NRPs are long-lived, persisting within poorly
338 differentiated carcinomas. Even so, we have not yet observed conditions under which murine
339 NRPs proliferate so as to constitute a significant population of carcinoma cells. It is possible
340 that NRPs being resistant to chemotherapy may be selected for confronted with treatment [21,
341 23], and possibly proliferate subsequently in that environment.

342 The coexistence of tuft cells and neuroendocrine cellular subpopulations is a
343 characteristic of several carcinoma types. Small cell lung cancer (SCLC) can be classified
344 into subtypes that include a tuft cell-like subtype based on POU2F3 expression and two
345 neuroendocrine subtypes based on ASCL1 and NEUROD1 expression [26]. Tuft cell-like SCLC
346 transitions to neuroendocrine subtypes as SCLC tumors lose *Tp53* and have an increased
347 activity of *Myc* [37]. In addition to this neural transition, these cells are characterized by the
348 gain of EMT markers in SCLC [35, 37]. Neuroendocrine prostate cancer (NEPC) NRPs are also
349 driven by *Myc* expression and *Tp53* deletion [38, 48]. In the setting of prostate cancer, NEPC is
350 derived from epithelial cells[36] in prostate adenocarcinoma after the treatment of hormone
351 therapy and is associated with worse outcomes [38].

352 In summary, our study reveals a novel type of transdifferentiation of metaplastic tuft
353 cells to neural-like progenitor cells, shifting their role from suppressing tumor progression
354 through their chemosensory function in early-stage disease, to being associated with poor

355 outcomes in the later stages after TNT. We found that the TNT requires *Myc* activity [49-51] and
356 possibly the loss of *Tp53* function[37], associations that have been observed in other tumor
357 types [27, 35-37]. While this does not settle the debate as to whether mTCs can act as tumor
358 progenitor cells, the NRP progeny of mTCs can persist long term as part of a poorly
359 differentiated carcinoma, though their lack of proliferation under unperturbed conditions
360 makes it unlikely that they contribute significantly to overall tumor burden. The observation
361 that NRPs are resistant to chemotherapy and their numbers are associated with worse
362 outcome and tumor recurrence[21, 23] suggest that, when challenged, their role may shift to a
363 more traditional tumor initiating cell. Other studies suggest that mNECs instead play a
364 supportive role for other carcinoma cells, promoting their expansion and possibly contributing
365 to their survival under stress [40], though whether these are functions common to both EECs
366 and NRPs has not been determined. While the specific functions of NRPs in PDA remain
367 under investigation, understanding the mechanisms controlling their genesis suggests that
368 one possible way to target these aggressive carcinoma cells is to reverse the TNT process to
369 restore their mTC tumor suppressing role.

370 **Methods**

371 *Mouse Models*

372 *mTC Lineage tracing*

373 *Pou2f3*$^{CreERT/+}$ [19], *ROSA26*$^{LSL\text{-}TdTomato/+}$ [28]. These were combined to generate
374 *Ptf1a*$^{FlpO/+}$*; FSF-KRAS*$^{G12D/+}$ [18, 52]*; Pou2f3*$^{CreERT/+}$ [19]*; ROSA26*$^{LSL\text{-}TdTomato/+}$ (*KF-P2f3T*) and
375 *Ptf1a*$^{FlpO/+}$*; FSF-KRAS*$^{G12D/+}$*; Trp53*$^{Frt\text{-}Exons\ 2\ to\ 5\text{-}Frt/+}$ [18, 52]*; Pou2f3*$^{CreERT/+}$ [19]*; ROSA26*$^{LSL\text{-}TdTomato/+}$
376 (*KPF-P2f3T*) mice. We induced pancreatic damage in the 8- to 9-week-old *KF-P2f3T* mice
377 with a once-daily intraperitoneal injection of cerulein (46-1-50; American Peptide Company,

378 Inc, Sunnyvale, CA) at a dose of 250 µg/kg for a total of five days. To induce recombination
379 of ROSA26$^{LSL\text{-}TdTomato/+}$ in *KF-P2f3T* and *KPF-P2f3T* models, 11- to 12-week-old mice were
380 treated with 5mg of Tamoxifen (T5648; Millipore-Sigma, St Louis, MO) via oral gavage, once
381 a day, for 5 days. Tamoxifen was dissolved in corn oil before treating mice. Pancreata were
382 then harvested 1-day post-tamoxifen, three days post-tamoxifen, and seven weeks post-
383 tamoxifen to capture different stages of PDA in mice.

384 *Acinar-derived mTCs and mNECs*

385 *Ptf1a^{Cre+}; LSL-KRAS$^{G12D/+}$; LSL-Trp53$^{R172H/+}$; ROSA26$^{LSL\text{-}YFP/+}$* [9] were combined to
386 generate *Ptf1a^{Cre+}; LSL-KRAS$^{G12D/+}$, ROSA26$^{LSL\text{-}YFP/+}$* (KCY) and *Ptf1a^{Cre+}; LSL-KRAS$^{G12D/+}$;*
387 *LSL-Trp53$^{R172H/+}$; ROSA26$^{LSL\text{-}YFP/+}$* (KPCY) mice to allow lineage trace of epithelial
388 compartment. KCY mice were treated with Cerulein at 9 weeks old and allowed to recover
389 for 3 weeks. KCY and KPCY mice were treated with Tamoxifen to induce YFP expression in
390 Ptf1a+ cells at twelve weeks of age.

391 *mTC Ablation*

392 A homozygous CreERT knock-in inserted into the *Pou2f3* locus was used to induce
393 metaplastic tuft cell ablation in KF and KPF mice. 8- to 9-week-old *Ptf1a$^{FlpO/+}$; FSF-*
394 *KRAS$^{G12D/+}$* [18, 52]*; Pou2f3$^{CreERT/CreERT}$* (KF; Pou2f3$^{CreERT/CreERT}$) mice were treated with cerulein
395 via intraperitoneal injection at a dose of 250 µg/kg for a total of 5 days to induce pancreatic
396 damage. *Ptf1a$^{FlpO/+}$; FSF-KRAS$^{G12D/+}$; Trp53$^{Frt\text{-}Exons\ 2\ to\ 5\text{-}Frt/+}$;* [18, 52] *Pou2f3$^{CreERT/CreERT}$* (KPF;
397 Pou2f3$^{CreERT/CreERT}$) did not require cerulein to cause damage. Pancreata were harvested at
398 12 weeks of age to determine ablation of mTCs in both models.

399

400 *cMyc overexpression in mTCs*

401 To Investigate the role of *cMyc* in the transdifferentiation of mTCs into mNECs, we
402 bred mouse lines to create the genotype: *Ptf1a*$^{FlpO/+}$, *KRAS*$^{FSF\text{-}G12D/+}$, *Pou2f3*$^{CreERT/+\ 16,\ 20}$,
403 *ROSA26*$^{LSL\text{-}TdTomato/+}$, *ROSA26* $^{LSL\text{-}cMyc/+\ 23}$. These were combined to generate KF-MOE mice
404 comprised of *Ptf1a*$^{FlpO/+}$; *FSF-KRAS*$^{G12D/+\ 18,\ 52}$; *Pou2f3*$^{CreERT/+\ 20}$; *ROSA26*$^{LSL\text{-}TdTomato/+}$;
405 *ROSA26* $^{LSL\text{-}cMyc/+\ 23}$. KF-MOE mice overexpressed *cMyc* and tdTomato reporter specifically
406 in mTCs in the KF neoplasia model. Pancreatic damage was induced in 8- to 9-week-old KF-
407 MOE mice with a once-daily intraperitoneal injection of cerulein (46-1-50; American Peptide
408 Company, Inc, Sunnyvale, CA) at a dose of 250 µg/kg for a total of 5 days. To induce
409 recombination of *ROSA26*$^{LSL\text{-}TdTomato/+}$ and *ROSA26*$^{LSL\text{-}cMyc/+\ 23}$ in the KF-MOE model, eleven-
410 to twelve-week-old mice were treated with 5mg of Tamoxifen (T5648; Millipore-Sigma, St
411 Louis, MO) via oral gavage, once a day, for 5 days. Tamoxifen was dissolved in corn oil
412 before treating mice. We harvested pancreata 3 days post-tamoxifen and seven weeks post-
413 tamoxifen to investigate the role of *cMyc* in mTC-derived mNECs.

414 *cMyc flox in mTCs*

415 To Investigate the role of *cMyc* in the transdifferentiation of mTCs into mNECs, we
416 bred mouse lines to create the genotype: *Ptf1a*$^{FlpO/+}$, *KRAS*$^{FSF\text{-}G12D/+}$, *Trp53*$^{Frt\text{-}Exons\ 2\ to\ 5\text{-}Frt/+\ 18,}$
417 ^{52}, *Pou2f3*$^{CreERT/+\ 16,\ 20}$, *ROSA26*$^{LSL\text{-}TdTomato/+}$, *Myc*$^{Flox/+\ 23}$. These were combined to generate
418 *KPF-P2M*$^{Fl/+}$ mice comprised of *Ptf1a*$^{FlpO/+}$; *FSF-KRAS*$^{G12D/+\ 18,\ 52}$; *Trp53*$^{Frt\text{-}Exons\ 2\ to\ 5\text{-}Frt/+}$
419 *Pou2f3*$^{CreERT/+\ 20}$; *ROSA26*$^{LSL\text{-}TdTomato/+}$; *Myc*$^{Flox/+\ 23}$. *KPF-P2M*$^{Fl/+}$ mice reduced *Myc* activity
420 and expressed the tdTomato reporter specifically in mTCs in the KPF PDA carcinoma model.
421 To induce recombination of *ROSA26*$^{LSL\text{-}TdTomato/+}$ and *Myc*$^{Flox/+\ 23}$ in the *KPF-P2M*$^{Fl/+}$ model,
422 eleven- to twelve-week-old mice were treated with 5mg of Tamoxifen (T5648; Millipore-

423 Sigma, St Louis, MO) via oral gavage, once a day, for 5 days. Tamoxifen was dissolved in
424 corn oil before treating mice. We harvested pancreata seven weeks post-tamoxifen to
425 investigate the role of *Myc* in mTC-derived mNECs.

426 *Immunohistochemistry (IHC)*

427 Mouse pancreas tissues were fixed overnight in a Z-fix solution (NC9050753; Anatech
428 Ltd, Battle Creek, MI). The pancreas tissues were processed using a Leica ASP300S tissue
429 processor (Buffalo Grove, IL). Sections (4 μm) of paraffin-embedded tissue were stained for
430 target proteins (Table 1) of interest using the Discovery Ultra XT auto Stainer (Ventana
431 Medical Systems Inc, Tucson, AZ). IHC slides were imaged and stitched together by a
432 3DHisTech scanner (Perkin Elmer, Seattle, WA) using a ×20 objective lens.

433 *Immunofluorescence (IF)*

434 Tissues were prepared as Z-fixed paraffin-embedded blocks, as stated above. In
435 increased dilutions, sectioned tissue was deparaffinized using xylene and a series of ethanol.
436 We boiled the slides in a pH 6.0 Citrate buffer solution for 5 minutes. Slides were allowed to
437 cool at room temperature for 20 mins, then washed in 0.1% tritonX + PBS solution for 15
438 mins three times for a total of 45 mins. The sections were then blocked in a donkey block
439 solution of 5% donkey serum/1% bovine serum albumin (BSA) in PBS for 1 hour. Following
440 the block, sections were incubated overnight with primary antibodies, as stated in **Supp.**
441 **Table 1.** The following day, we washed in a 0.1% TritonX + PBS solution for 15 mins thrice.
442 Then Alexa Fluor-conjugated secondary antibodies (1:500, Invitrogen, Carlsbad, CA) were
443 added and incubated at RT for 1hr in the dark. Slides were then washed once more with
444 0.1% TritonX + PBS + Hoechst 33342 (62249, 1:10000, Thermo Scientific, Carlsbad, CA)
445 solution for 15 mins thrice to remove excess secondary and label nuclei. Lastly, slides were

446 briefly rinsed in deionized water, mounted with Prolong Diamond antifade mountant (P36961;
447 Fisher), and dried overnight at room temperature before imaging.

448 *EdU Proliferation Assay:*

449 The "Click-iT™ Plus EdU Cell Proliferation Kit for Imaging, Alexa Fluor™ 488 dye"
450 (ThermoFisher, Catalog number: C10637) was used to label cells that have undergone
451 proliferation for a specific time period [53]. We dissolved EdU in PBS to a concentration of
452 1mg/mL. *KPF-P2f3T* mice were treated with tamoxifen at 11- to 12- weeks of age once daily
453 for 5 days. Mice were treated with 100uL of EdU injected via I.P. injection every 12 hours for
454 3 days post tamoxifen labeling. We harvested the pancreata from each mouse the following
455 morning. We fixed and stained each pancreas as mentioned in the IF protocol above just
456 until after secondary antibodies were added and washed in 0.1% TritonX + PBS + Hoechst
457 33342 (62249, 1:10000, Thermo Scientific, Carlsbad, CA) solution for 15 mins three times to
458 removed excess secondary and label nuclei. We detected EdU by making a cocktail using
459 the following components provided by the kit: 440uL of 1x Click-iT Reaction buffer, 10uL of
460 Copper Protectant, 1.2uL of Alexa Fluor Picolyl, and 50uL of Reaction buffer additive.
461 Reagents must be added in the order listed. 100uL of the cocktail was added to each slide
462 and incubated for 30 minutes before washing with 3% BSA in PBS. We rinsed the slides with
463 ddH2O, mounted them with Prolong Diamond antifade mountant (P36961; Fisher), and dried
464 them overnight at room temperature before imaging.

465 *Quantitation*

466 HALO Software (Indica Labs, Corrales, NM) was used to quantify whole tissue
467 scanned sections. Quantification excluded blood vessels, lymph nodes, and
468 adipose/connective tissue. We took multiple sections from each tissue throughout the block

469 and averaged them to produce a data point. Through this software, we can train the
470 algorithm to recognize specific areas of tissue and allow us to determine marker expression
471 in different regions of the pancreas using the whole section. We did image analysis as per
472 Indica Labs' recommendations.

473 **Acknowledgements**

474 The authors would like to thank Marina Pasca di Magliano for helpful discussions. This work
475 was supported by R01CA235141, U01CA224145 and U01CA274154 (to HCC). DJSE was
476 supported by the University of Michigan's Rackham Merit Fellowship, NCI F31CA271576,
477 and NCI T32CA009676. KED is supported by the Vanderbilt Ingram Cancer Center Support
478 Grant (NIH/NCI P30CA068485), the Vanderbilt-Ingram Cancer Center SPORE in
479 Gastrointestinal Cancer (NIH/NCI P50CA236733), the Vanderbilt Digestive Disease
480 Research Center (NIH/NIDDK P30DK058404), an American Gastroenterological Association
481 Research Scholar Award (AGA2021-13-02), NIH/NIGMS R35GM142709, The Department of
482 Defense (DOD W81XWH2211121), The Sky Foundation, Inc (AWD00000079), and Linda's
483 Hope (Nashville, TN). RCS is supported by: NCI U01CA224012 and R01s CA186241,
484 CA196228 and DoD PA210068. SB was supported by a postdoctoral fellowship from the
485 German Research Foundation (BE 7224/1-1) and a research grant provided by the Sky
486 Foundation. NGS is supported by NCI R00 CA263154 and the Henry Ford Health + Michigan
487 State University Collaboration grant.

References:

1. Society, A.C., *Cancer Facts & Figures 2024.* American Cancer Society, 2024.
2. Chu, L.C., M.G. Goggins, and E.K. Fishman, *Diagnosis and Detection of Pancreatic Cancer.* The Cancer Journal, 2017. **23**(6): p. 333-342.
3. Pihlak, R., J. Weaver, J. Valle, and M. McNamara, *Advances in Molecular Profiling and Categorisation of Pancreatic Adenocarcinoma and the Implications for Therapy.* Cancers, 2018. **10**(1): p. 17.
4. Sahin, I.H., C.A. Iacobuzio-Donahue, and E.M. O'Reilly, *Molecular signature of pancreatic adenocarcinoma: an insight from genotype to phenotype and challenges for targeted therapy.* Expert Opinion on Therapeutic Targets, 2016. **20**(3): p. 341-359.
5. *Pancreatic Cancer: Molecular Characterization, Clonal Evolution and Cancer Stem Cells.* Biomedicines, 2017. **5**(4): p. 65.
6. Benitz, S.*, et al.*, *ROR2 regulates cellular plasticity in pancreatic neoplasia and adenocarcinoma*. 2023, Cold Spring Harbor Laboratory.
7. Schlesinger, Y.*, et al.*, *Single-cell transcriptomes of pancreatic preinvasive lesions and cancer reveal acinar metaplastic cells' heterogeneity.* Nature Communications, 2020. **11**(1).
8. Delgiorno, K.E.*, et al.*, *Tuft Cells Inhibit Pancreatic Tumorigenesis in Mice by Producing Prostaglandin D2.* Gastroenterology, 2020. **159**(5): p. 1866-1881.e8.
9. Delgiorno, K.E.*, et al.*, *Identification and Manipulation of Biliary Metaplasia in Pancreatic Tumors.* Gastroenterology, 2014. **146**(1): p. 233-244.e5.
10. Hoffman, M.T.*, et al.*, *The Gustatory Sensory G-Protein GNAT3 Suppresses Pancreatic Cancer Progression in Mice.* Cellular and Molecular Gastroenterology and Hepatology, 2021. **11**(2): p. 349-369.
11. Bailey, J.M.*, et al.*, *DCLK1 Marks a Morphologically Distinct Subpopulation of Cells With Stem Cell Properties in Preinvasive Pancreatic Cancer.* Gastroenterology, 2014. **146**(1): p. 245-256.
12. Nevo, S., N. Kadouri, and J. Abramson, *Tuft cells: From the mucosa to the thymus.* Immunology Letters, 2019. **210**: p. 1-9.
13. Hoover, B., V. Baena, M.M. Kaelberer, F. Getaneh, S. Chinchilla, and D.V. Bohórquez, *The intestinal tuft cell nanostructure in 3D.* Scientific Reports, 2017. **7**(1).
14. Howitt, M.R.*, et al.*, *Tuft cells, taste-chemosensory cells, orchestrate parasite type 2 immunity in the gut.* Science, 2016. **351**(6279): p. 1329-1333.
15. Yamashita, J., M. Ohmoto, T. Yamaguchi, I. Matsumoto, and J. Hirota, *Skn-1a/Pou2f3 functions as a master regulator to generate Trpm5-expressing chemosensory cells in mice.* PLOS ONE, 2017. **12**(12): p. e0189340.
16. Yamaguchi, T.*, et al.*, *Skn-1a/Pou2f3 is required for the generation of Trpm5-expressing microvillous cells in the mouse main olfactory epithelium.* BMC Neuroscience, 2014. **15**(1): p. 13.
17. Ma, Z.*, et al.*, *Single-Cell Transcriptomics Reveals a Conserved Metaplasia Program in Pancreatic Injury.* Gastroenterology, 2022. **162**(2): p. 604-620 e20.
18. Garcia, P.E.*, et al.*, *Differential Contribution of Pancreatic Fibroblast Subsets to the Pancreatic Cancer Stroma.* Cell Mol Gastroenterol Hepatol, 2020. **10**(3): p. 581-599.
19. McGinty, J.W., H.-A. Ting, T.E. Billipp, M.S. Nadjsombati, D.M. Khan, N.A. Barrett, H.-E. Liang, I. Matsumoto, and J. Von Moltke, *Tuft-Cell-Derived Leukotrienes Drive Rapid Anti-helminth Immunity in the Small Intestine but Are Dispensable for Anti-protist Immunity.* Immunity, 2020. **52**(3): p. 528-541.e7.
20. Matsumoto, I., M. Ohmoto, M. Narukawa, Y. Yoshihara, and K. Abe, *Skn-1a (Pou2f3) specifies taste receptor cell lineage.* Nature Neuroscience, 2011. **14**(6): p. 685-687.
21. Hwang, W.L.*, et al.*, *Single-nucleus and spatial transcriptome profiling of pancreatic cancer identifies multicellular dynamics associated with neoadjuvant treatment.* Nature Genetics, 2022. **54**(8): p. 1178-1191.

538 22. Caplan, L.R., V. Vavinskaya, D.G. Gelikman, N. Jyotsana, V.Q. Trinh, K.P. Olive, M.C.B. Tan,
539 and K.E. Delgiorno, *Enteroendocrine Cell Formation Is an Early Event in Pancreatic*
540 *Tumorigenesis.* Frontiers in Physiology, 2022. **13**.
541 23. Farrell, A.S.*, et al.*, *MYC regulates ductal-neuroendocrine lineage plasticity in pancreatic*
542 *ductal adenocarcinoma associated with poor outcome and chemoresistance.* Nature
543 Communications, 2017. **8**(1).
544 24. Wu, C.-Y.C.*, et al.*, *PI3K Regulation of RAC1 Is Required for KRAS-Induced Pancreatic*
545 *Tumorigenesis in Mice.* Gastroenterology, 2014. **147**(6): p. 1405-1416.e7.
546 25. Wen, H.-J., S. Gao, Y. Wang, M. Ray, M.A. Magnuson, C.V.E. Wright, M.P. Di Magliano, T.L.
547 Frankel, and H.C. Crawford, *Myeloid Cell-Derived HB-EGF Drives Tissue Recovery After*
548 *Pancreatitis.* Cellular and Molecular Gastroenterology and Hepatology, 2019. **8**(2): p. 173-192.
549 26. Baine, M.K.*, et al.*, *SCLC Subtypes Defined by ASCL1, NEUROD1, POU2F3, and YAP1: A*
550 *Comprehensive Immunohistochemical and Histopathologic Characterization.* Journal of
551 Thoracic Oncology, 2020. **15**(12): p. 1823-1835.
552 27. Huang, Y.-H.*, et al.*, *POU2F3 is a master regulator of a tuft cell-like variant of small cell lung*
553 *cancer.* Genes & Development, 2018. **32**(13-14): p. 915-928.
554 28. Madisen, L.*, et al.*, *A robust and high-throughput Cre reporting and characterization system for*
555 *the whole mouse brain.* Nat Neurosci, 2010. **13**(1): p. 133-40.
556 29. Burclaff, J., S.G. Willet, J.B. Sáenz, and J.C. Mills, *Proliferation and Differentiation of Gastric*
557 *Mucous Neck and Chief Cells During Homeostasis and Injury-induced Metaplasia.*
558 Gastroenterology, 2020. **158**(3): p. 598-609.e5.
559 30. Westphalen, C.B.*, et al.*, *Dclk1 Defines Quiescent Pancreatic Progenitors that Promote Injury-*
560 *Induced Regeneration and Tumorigenesis.* Cell Stem Cell, 2016. **18**(4): p. 441-455.
561 31. Worthington, J.J., F. Reimann, and F.M. Gribble, *Enteroendocrine cells-sensory sentinels of*
562 *the intestinal environment and orchestrators of mucosal immunity.* Mucosal Immunology,
563 2018. **11**(1): p. 3-20.
564 32. Riedel, M.J., A. Asadi, R. Wang, Z. Ao, G.L. Warnock, and T.J. Kieffer, *Immunohistochemical*
565 *characterisation of cells co-producing insulin and glucagon in the developing human pancreas.*
566 Diabetologia, 2012. **55**(2): p. 372-381.
567 33. Hu, L.*, et al.*, *Genome-Wide Association Study of Prognosis in Advanced Non–Small Cell*
568 *Lung Cancer Patients Receiving Platinum-Based Chemotherapy.* Clinical Cancer Research,
569 2012. **18**(19): p. 5507-5514.
570 34. Lim, U.*, et al.*, *Susceptibility variants for obesity and colorectal cancer risk: The multiethnic*
571 *cohort and PAGE studies.* International Journal of Cancer, 2012. **131**(6): p. E1038-E1043.
572 35. Ireland, A.S.*, et al.*, *MYC Drives Temporal Evolution of Small Cell Lung Cancer Subtypes by*
573 *Reprogramming Neuroendocrine Fate.* Cancer Cell, 2020. **38**(1): p. 60-78.e12.
574 36. Lee, J.K.*, et al.*, *N-Myc Drives Neuroendocrine Prostate Cancer Initiated from Human Prostate*
575 *Epithelial Cells.* Cancer Cell, 2016. **29**(4): p. 536-547.
576 37. Mollaoglu, G.*, et al.*, *MYC Drives Progression of Small Cell Lung Cancer to a Variant*
577 *Neuroendocrine Subtype with Vulnerability to Aurora Kinase Inhibition.* Cancer Cell, 2017.
578 **31**(2): p. 270-285.
579 38. Yin, Y.*, et al.*, *N-Myc promotes therapeutic resistance development of neuroendocrine prostate*
580 *cancer by differentially regulating miR-421/ATM pathway.* Molecular Cancer, 2019. **18**(1).
581 39. Barker, N., *Adult intestinal stem cells: critical drivers of epithelial homeostasis and*
582 *regeneration.* Nature Reviews Molecular Cell Biology, 2014. **15**(1): p. 19-33.
583 40. Sinha, S.*, et al.*, *PanIN Neuroendocrine Cells Promote Tumorigenesis via Neuronal Cross-talk.*
584 Cancer Research, 2017. **77**(8): p. 1868-1879.
585 41. Koga, H., Y. Ikezono, and T. Torimura, *Pancreatic DCLK1 marks quiescent but oncogenic*
586 *progenitors: a possible link to neuroendocrine tumors.* Stem Cell Investigation, 2016. **3**: p. 37-
587 37.
588 42. Nakanishi, Y.*, et al.*, *Dclk1 distinguishes between tumor and normal stem cells in the intestine.*
589 Nature Genetics, 2013. **45**(1): p. 98-103.

43. Saqui-Salces, M., T.M. Keeley, A.S. Grosse, X.T. Qiao, M. El-Zaatari, D.L. Gumucio, L.C. Samuelson, and J.L. Merchant, *Gastric tuft cells express DCLK1 and are expanded in hyperplasia.* Histochemistry and Cell Biology, 2011. **136**(2): p. 191-204.
44. Nawabi, H.*, et al.*, *Doublecortin-Like Kinases Promote Neuronal Survival and Induce Growth Cone Reformation via Distinct Mechanisms.* Neuron, 2015. **88**(4): p. 704-719.
45. May, R.*, et al.*, *Identification of a novel putative pancreatic stem/progenitor cell marker DCAMKL-1 in normal mouse pancreas.* Am J Physiol Gastrointest Liver Physiol, 2010. **299**(2): p. G303-10.
46. Xu, L., M. Zhang, L. Shi, X. Yang, L. Chen, N. Cao, A. Lei, and Y. Cao, *Neural stemness contributes to cell tumorigenicity.* Cell & Bioscience, 2021. **11**(1).
47. Zhang, Z.*, et al.*, *Similarity in gene-regulatory networks suggests that cancer cells share characteristics of embryonic neural cells.* Journal of Biological Chemistry, 2017. **292**(31): p. 12842-12859.
48. Beltran, H.*, et al.*, *The role of lineage plasticity in prostate cancer therapy resistance.* Clinical Cancer Research, 2019: p. clincanres.1423.
49. Dai, M.-S., Y. Jin, J.R. Gallegos, and H. Lu, *Balance of Yin and Yang: Ubiquitylation-Mediated Regulation of p53 and c-Myc.* Neoplasia, 2006. **8**(8): p. 630-644.
50. Feng, Y.C.*, et al.*, *c-Myc inactivation of p53 through the pan-cancer lncRNA MILIP drives cancer pathogenesis.* Nature Communications, 2020. **11**(1).
51. Ho, J.S.L., W. Ma, D.Y.L. Mao, and S. Benchimol, *p53-Dependent Transcriptional Repression of c-myc Is Required for G₁ Cell Cycle Arrest.* Molecular and Cellular Biology, 2005. **25**(17): p. 7423-7431.
52. Wu, J.*, et al.*, *Generation of a pancreatic cancer model using a Pdx1-Flp recombinase knock-in allele.* PLOS ONE, 2017. **12**(9): p. e0184984.
53. Zhang, H.*, et al.*, *Glucose-Mediated Repression of Menin Promotes Pancreatic β-Cell Proliferation.* Endocrinology, 2012. **153**(2): p. 602-611.

618 **Figure Legends:**

619 **Figure 1. Lineage trace model shows tuft cell specific expression of tdTomato.**

620 Genetic strategy to trace the fate of metaplastic tuft cells (mTCs) in pancreatic cancer progression
621 using a dual recombinase neoplasia (*KF-P2f3T*) model **(A)** and carcinoma (*KPF-P2f3T*) model **(B)**. **C)**
622 Treatment regimen for neoplasia and carcinoma Models. The models have both pancreatic
623 progression and reporter specifically in tuft cells. The *KF-P2f3T* model utilizes Cerulein once daily,
624 followed by 2 weeks recovery, then once daily tamoxifen treatment for 5 days. The *KPF-P2f3T* model
625 is aggressive as it contains one null p53 allele. Cerulein is not necessary and so only Tamoxifen is
626 treated once daily for 5 days. Mice are allowed to age for different time points to determine lineage of
627 metaplastic tuft cells in progression of pancreatic cancer. **D)** Dclk1 in Brown identifies tuft cells in
628 neoplasia model (left) and carcinoma model (right). **E)** Specific expression of tdTomato reporter in
629 both models. White represents Hoechst staining to mark the nucleus, tdTomato in red to show
630 recombination of tdTomato (tdTom), Pou2f3, the master regulator of tuft cells in Green, and
631 Acetylated alpha tubulin in Magenta to mark filamentous actin in the tufts of the mTCs. **F)** Dual IHC of
632 tdTom (Teal) and CC3 (Brown) stained *KF-P2f3T* and *KPF-P2f3T* mice to determine cell death of
633 mTCs in neoplasia and carcinoma. Black arrows indicate tdTom+ cells in lesions. Scale bars = 10 μm
634 unless otherwise noted.

635

636 **Figure 2. Lineage tracing mTCs reveals transdifferentiation to metaplastic neuroendocrine**
637 **cells (mNECs).**

638 Dual recombinase models show fate of mTCs in progression of pancreatic cancer. **A)** Mice harvested
639 3 days post-tamoxifen treatment for labeling mTCs. Hoechst stains nucleus of cells (White), Cox1 is
640 used to identify mTCs (Green), tdTom reporter to determine fate of mTCs (Red) and acetylated-α-
641 tubulin (Magenta) marks filamentous actin on tuft of mTCs. **B)** Quantification of Percentage of mTC
642 (White) and mTC Progeny (Pink) among ductal cells at different time points post-tamoxifen treatment

643 in *KF-P2f3T* and *KPF-P2f3T* models. mTCs are identified by Cox1 and tdTom, mTC Progeny are only
644 tdTom positive. (n = 3/group) p-values were calculated using a two-way ANOVA on Prism GraphPad
645 7. * = $p < 0.05$, ** = $p < 0.01$. **C)** Co-staining of tdTomato (Red) expression with remaining
646 metaplastic ductal cell subsets. In Green, Gkn1, Lectin GS-II, and Synaptophysin (Syp) mark gastric
647 pit-like, gastric neck-like, and neuroendocrine cells respectively in pancreatic metaplastic ducts. **D)** 7
648 weeks post-tamoxifen labeling of neoplasia and carcinoma models exposes shift of populations.
649 Cox1 (Green) marks mTCs, tdTomato (Red) identifies reporter, Syp (White) marks neuroendocrine
650 cells, and Blue represents DAPI Staining to identify the nucleus of a cell. **E)** Quantification of
651 percentage of mTCs (Cox1+ tdTom+) in White, mTC-derived mNECs (Syp+ tdTom+) in Pink, mTC-
652 independent mNECs (Syp+ tdTom-) in Green. (n = 3/group). p-values were calculated using a two-
653 way ANOVA on Prism GraphPad 7. * = $p < 0.05$, ** = $p < 0.01$. Scale bars = 10 μm unless otherwise
654 noted.

655

656 **Figure 3. Characterizing the tuft cell to neuroendocrine cell transdifferentiation (TNT).**

657 IF staining of Cox1 (Red) and Syp (Green) in neoplasia and carcinoma models determines that
658 mNECs in the *KPF-P2f3T* model relies on the mTC population. **A)** Cox1 (Red) and Syp (Green)
659 markers are stained in Pou2f3 double knock-in models of pancreatic neoplasia and carcinoma: (Left)
660 KF; Pou2f3$^{CreERT/CreERT}$ and (Right) KPF; Pou2f3$^{CreERT/CreERT}$, correspondingly to investigate the role of
661 tuft cells in mNEC genesis. Green Arrows denote mNECs, Red Asterisks denote stromal Cox1^{+}
662 staining identifying Cox1^{+} Immune cells. **B)** Pou2f3, the master regulator of tuft cells (Cyan) is stained
663 with Cox1, marker of tuft cells (Red), and Syp, neuroendocrine marker (Green) to determine if mNECs
664 also express Pou2f3. **C)** Dual IHC of Syp (Teal) and Ki67 (Brown) of neoplasia and carcinoma models
665 of pancreas to determine proliferation of mNECs. **D)** Co-IF of mTC marker, Cox1 (Green), lineage
666 tracer, tdTom (Red), mNEC marker, Syp (White), incorporated EdU (Magenta) to mark proliferating
667 cells, and nuclear marker, Hoechst (Blue) in *KPF-P2f3T* mice treated with EdU over the course of 3

668 days post-tamoxifen treatment. **E)** Yellow arrows mark rare transitionary cells that are marked with
669 both Syp (Green) and Cox1 (Red). Green arrow identifies cells that are only expressing Syp, mNECs.
670 Red arrow marks cells only expressing Cox1, mTCs. Scale bars = 10 μm unless otherwise noted.

671

672 **Figure 4. Identifying distinctions between mNECs in the progression of PDA.**

673 Neoplasia and carcinoma PDA models were stained with markers of different islet compartments to
674 determine differences between mNECs between the *KF-P2f3T* and *KPF-P2f3T* models. **B)** Islets and
675 lesions from *KF-P2f3T* and *KPF-P2f3T* are shown to determine co-localization of Syp (Red) and
676 markers of the different compartments of the Islet (Green). PanCK (Cyan) was used to distinguish
677 islet cells from mNECs, and Hoechst was used to mark the nucleus of each cell. Glucagon (Gcg),
678 Insulin (Ins), Somatostatin (Sst), Ghrelin (Ghrl), and Pancreatic Polypeptide (Pp) were stained to
679 identify the α cells, β cells, δ cells, ε cells and γ cells respectively. Scale bars = 10 μm unless
680 otherwise noted.

681

682 **Figure 5. mTC-derived mNECs are identified in PDA Carcinoma.**

683 IHC and IF are used to confirm the identity of mTC Progeny in dedifferentiated carcinoma of *KPF-*
684 *P2f3T* model. **A)** IHC of dedifferentiated carcinoma stained with Dclk1 (*Left*) and tdTomato (*Right*) in
685 Brown. **B)** Dedifferentiated carcinoma of *KPF-P2f3T* model is stained with Hoechst (Cyan), Syp
686 (White), and tdTomato (Red) to determine identity of mTC progeny. Scale bars = 50 μm

687

688

689

690

691 **Figure 6. Identification of mTC-derived Nrxn3+ NRPs in Carcinoma**

692 Co-staining of Syp (Red), Nrxn3 (Green), PanCK (Magenta), and Hoechst (White) in *KF-P2f3T*
693 neoplasia model and *KPF-P2f3T* carcinoma model at **A)** 3 days post-tamoxifen, **B)** 7 weeks post-
694 tamoxifen, and **C)** *KPF-P2f3T* dedifferentiated carcinoma. Scale bars = 10 µm unless otherwise
695 noted.

696 **Figure 7. cMyc Mediated development of mNECs.**

697 Overexpression and knockdown of *Myc* in neoplasia and carcinoma models show dependence of *Myc*
698 expression on transition of mTCs to NRPs in PDA progression. **A)** *KF-MOE* 7 weeks post-tamoxifen
699 treatment are stained with tdTom to identify cells recombined by tamoxifen treatment and cells
700 overexpressing *Myc* (Red), Syp to mark neuroendocrine cells (Green), Acetylated-α-tubulin to mark
701 filamentous actin of cells (Magenta), and Hoechst to identify nucleus of all cells (White) to detect
702 mTC-derived mNECs. **B)** KF-MOE 7 weeks post-tamoxifen treatment tissue is stained for co-IF to
703 determine expression of Syp (Green), tdTom (Red), Nrxn3 (Magenta), and Hoechst (White). **C)**
704 Quantification of mTCs (Cox1+ tdTom+) in White, mTC derived mNECs (Syp+ tdTom+) in Pink and
705 mTC independent mNECs (Syp+ tdTom-) in Green for *KF-P2f3T* and *KF-MOE* models. Mice were
706 sac'd after 3 days and 7 weeks post tamoxifen treatment to label tuft cells with tdTomato and
707 overexpress cMyc specifically in tuft cells. (n = 3/group) p-values were calculated using a two-way
708 ANOVA on Prism GraphPad 7. * = $p < 0.05$. D) Quantification of mTCs (White), mTC Derived
709 mNECs (Pink), and mTC Independent, (Green) in *KPF-P2f3T* and *KPF-P2M*$^{Fl/+}$ models. Mice were
710 sac'd at 7 weeks post tamoxifen treatment to label tuft cells with tdTom and flox *cMyc* expression in
711 tuft cells specifically. (n = 3/group) p-values were calculated using a two-way ANOVA on Prism
712 GraphPad 7. * = $p < 0.05$, **= $p<0.005$. **E)** Co-staining of Cox1 (Green), tdTom (Red), PanCK
713 (Magenta), and Hoechst (White) in *KPF-P2M*$^{Fl/+}$ at 7 weeks post-tamoxifen treatment to identify co-
714 localization of mTC marker, Cox1, with tdTom (*Top*). Co-staining of combined antibodies for Ghrl,

715 Gcg, Sst, Ppy, and Ins to mark cells expressing “Hormones” to identify EECs (Green), tdTom used to
716 identify cells recombined and *Myc* knockout cells (Red), PanCK to mark pancreatic epithelium/lesions
717 (Magenta), and Hoechst to mark nucleus of cells (White) in *KPF-P2M*$^{Fl/+}$ at 7 weeks post-tamoxifen
718 treatment to identify EECs and tdTom+ cells as separate cell populations when *Myc* is conditionally
719 knocked out in carcinoma model. Scale bars = 10 μm unless otherwise noted.

Figure 1

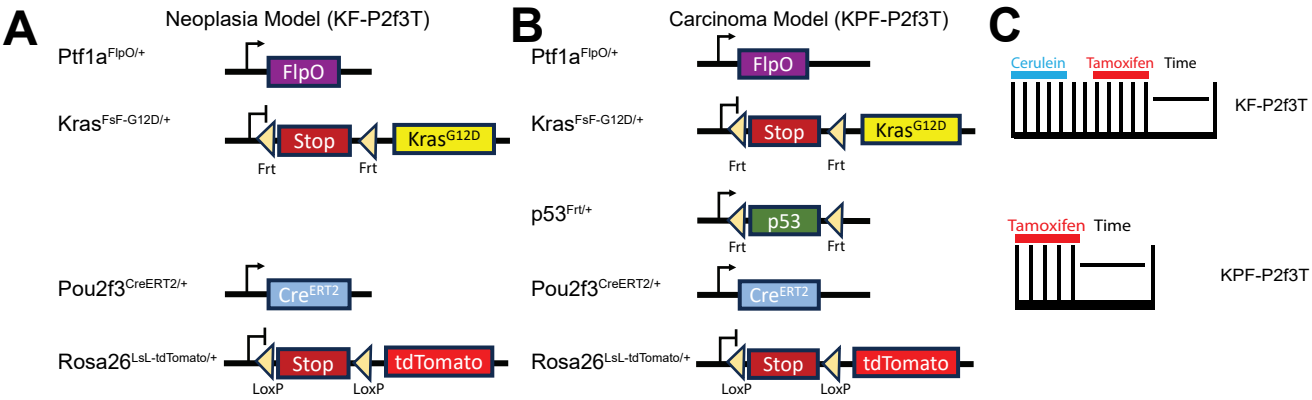
A
Neoplasia Model (KF-P2f3T)
Ptf1a FlpO/+
FlpO
Kras FsF-G12D/+
Stop
Kras G12D
Frt
Frt
Pou2f3 CreERT2/+
Cre ERT2
Rosa26 LsL-tdTomato/+
Stop
tdTomato
LoxP
LoxP
B
Carcinoma Model (KPF-P2f3T)
Ptf1a FlpO/+
FlpO
Kras FsF-G12D/+
Stop
Kras G12D
Frt
Frt
p53 Frt/+
p53
Frt
Frt
Pou2f3 CreERT2/+
Cre ERT2
Rosa26 LsL-tdTomato/+
Stop
tdTomato
LoxP
LoxP
C
Cerulein
Tamoxifen
Time
KF-P2f3T
Tamoxifen
Time
KPF-P2f3T

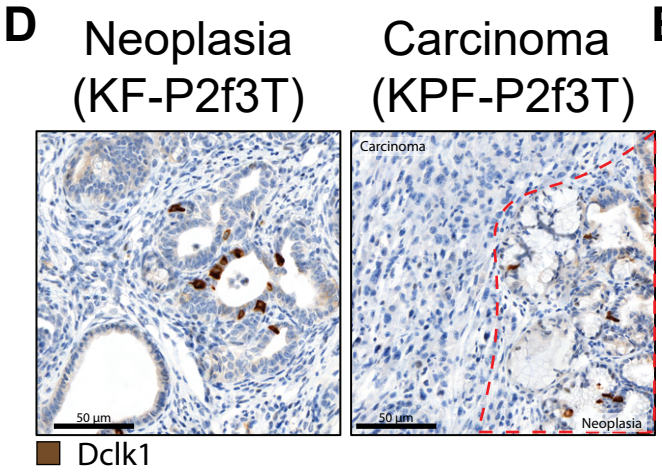
D
Neoplasia (KF-P2f3T)
Carcinoma (KPF-P2f3T)
Carcinoma
Neoplasia
50 µm
50 µm
Dclk1

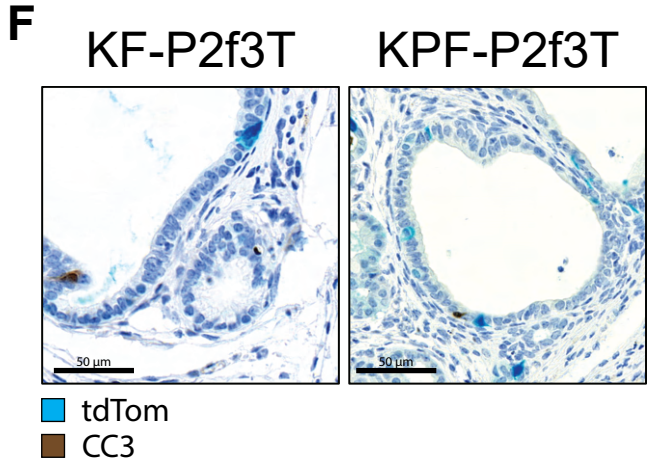
F
KF-P2f3T
KPF-P2f3T
50 µm
50 µm
tdTom
CC3

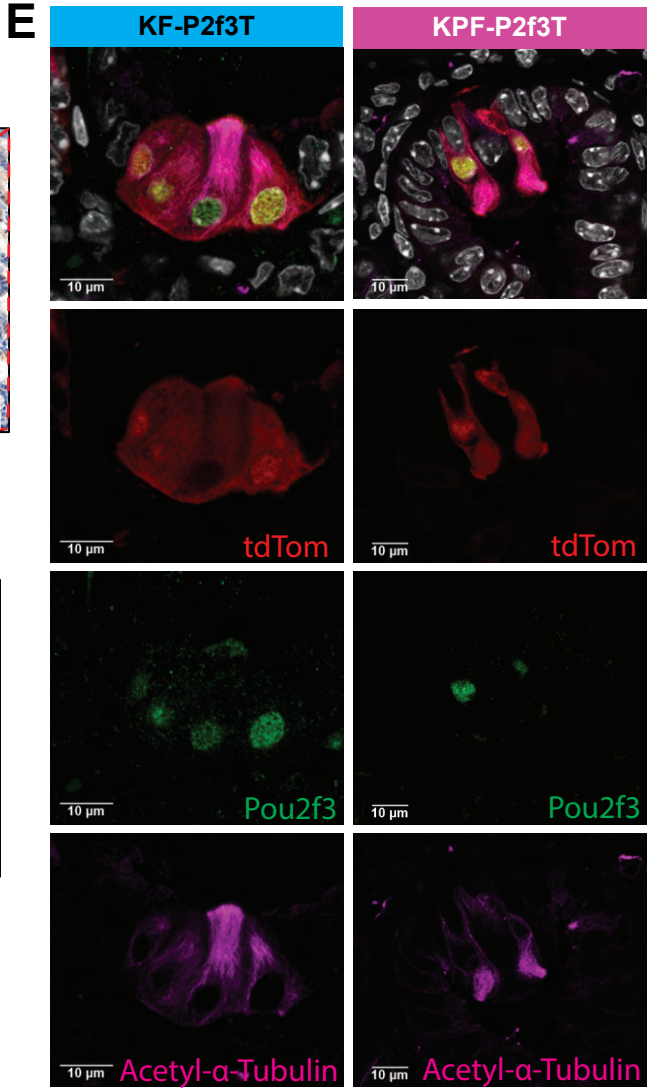
E
KF-P2f3T
KPF-P2f3T
10 µm
tdTom
Pou2f3
Acetyl-α-Tubulin

Figure 2

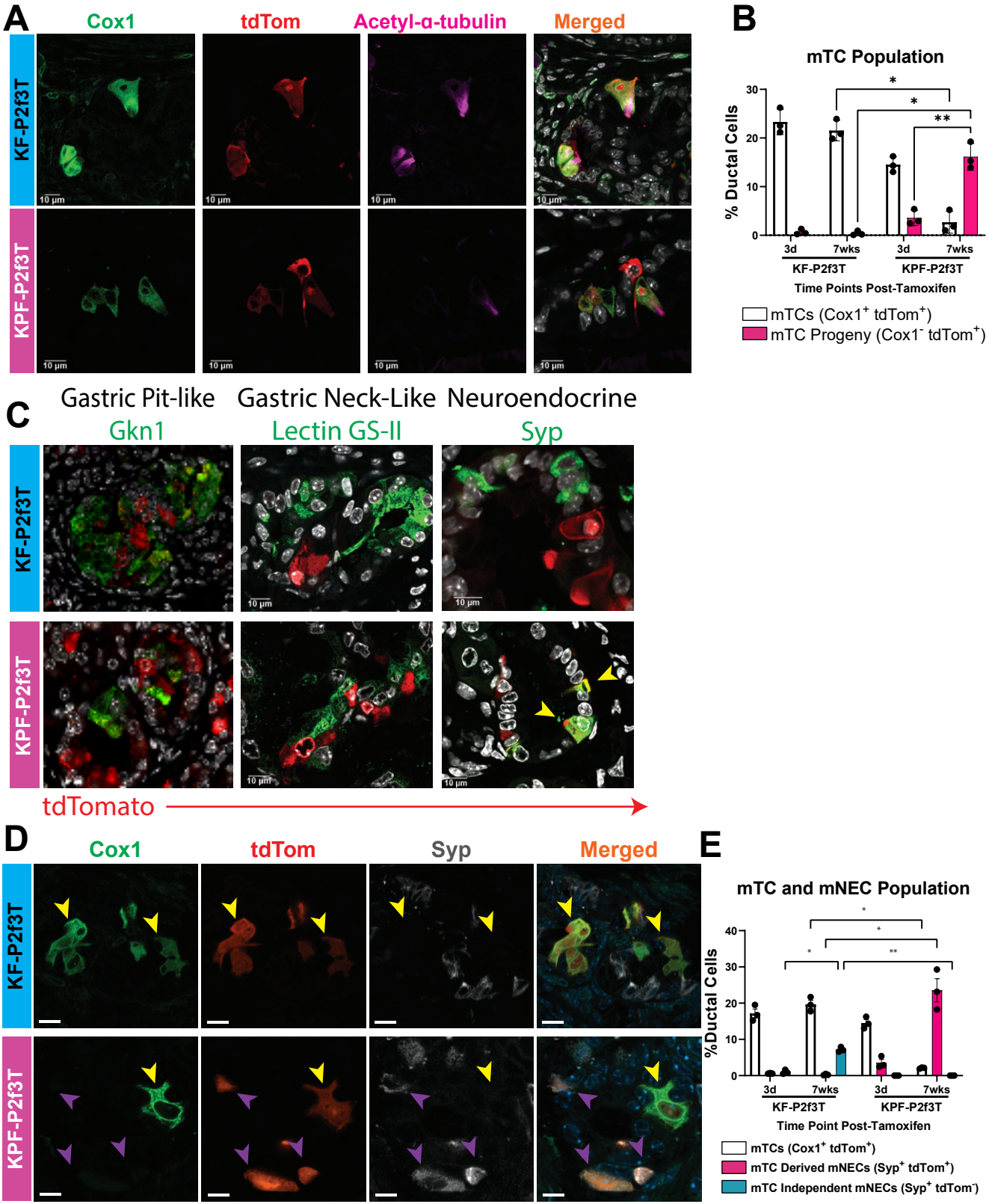
A
Cox1
tdTom
Acetyl-α-tubulin
Merged
KF-P2f3T
KPF-P2f3T
10 µm
B
mTC Population
% Ductal Cells
30
20
10
0
*
*
**
3d
7wks
3d
7wks
KF-P2f3T
KPF-P2f3T
Time Points Post-Tamoxifen
mTCs (Cox1+ tdTom+)
mTC Progeny (Cox1- tdTom+)
C
Gastric Pit-like
Gastric Neck-Like
Neuroendocrine
Gkn1
Lectin GS-II
Syp
KF-P2f3T
KPF-P2f3T
tdTomato
D
Cox1
tdTom
Syp
Merged
KF-P2f3T
KPF-P2f3T
E
mTC and mNEC Population
%Ductal Cells
40
30
20
10
0
*
*
*
**
3d
7wks
3d
7wks
KF-P2f3T
KPF-P2f3T
Time Point Post-Tamoxifen
mTCs (Cox1+ tdTom+)
mTC Derived mNECs (Syp+ tdTom+)
mTC Independent mNECs (Syp+ tdTom-)

Figure 3

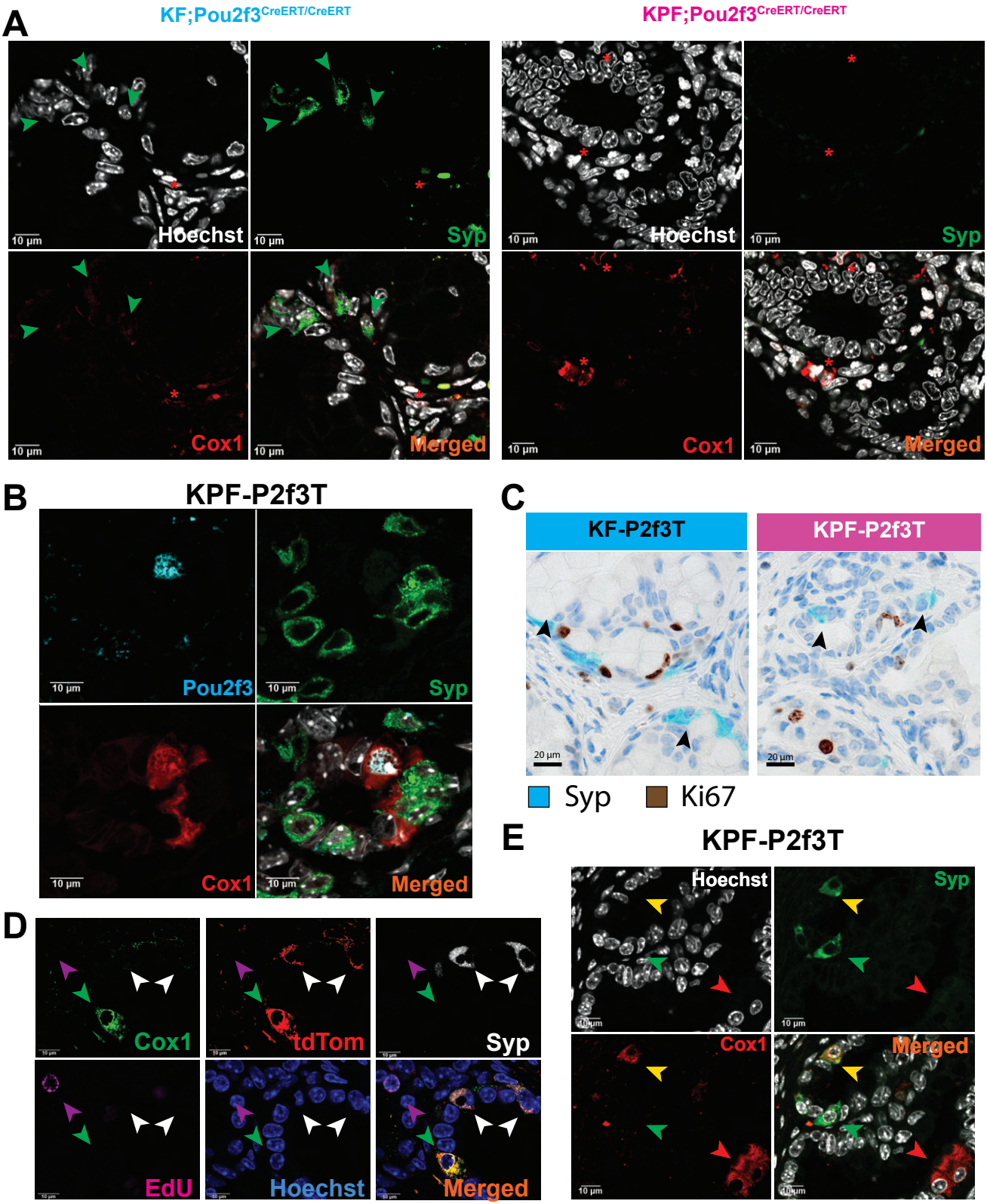
A
KF;Pou2f3CreERT/CreERT
KPF;Pou2f3CreERT/CreERT
Hoechst
Syp
Cox1
Merged
10 µm
B
KPF-P2f3T
Pou2f3
Syp
Cox1
Merged
10 µm
C
KF-P2f3T
KPF-P2f3T
20 µm
Syp
Ki67
D
Cox1
tdTom
Syp
EdU
Hoechst
Merged
E
KPF-P2f3T
Hoechst
Syp
Cox1
Merged
10 µm

Figure 4

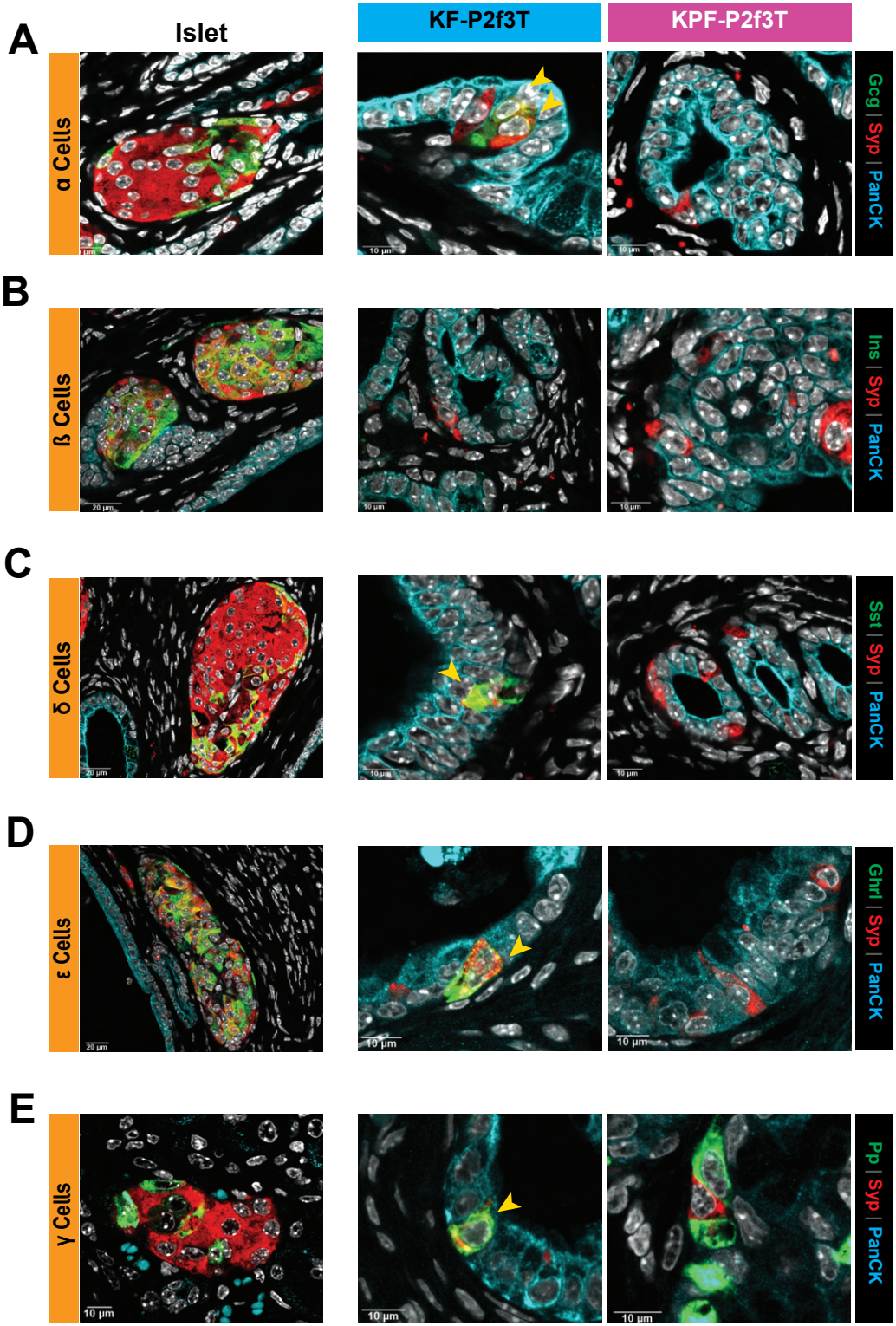
A
Islet
KF-P2f3T
KPF-P2f3T
α Cells
Gcg | Syp | PanCK
B
ß Cells
Ins | Syp | PanCK
C
δ Cells
Sst | Syp | PanCK
D
ε Cells
Ghrl | Syp | PanCK
E
γ Cells
Pp | Syp | PanCK
10 µm

Figure 5

A **KPF-P2f3T**

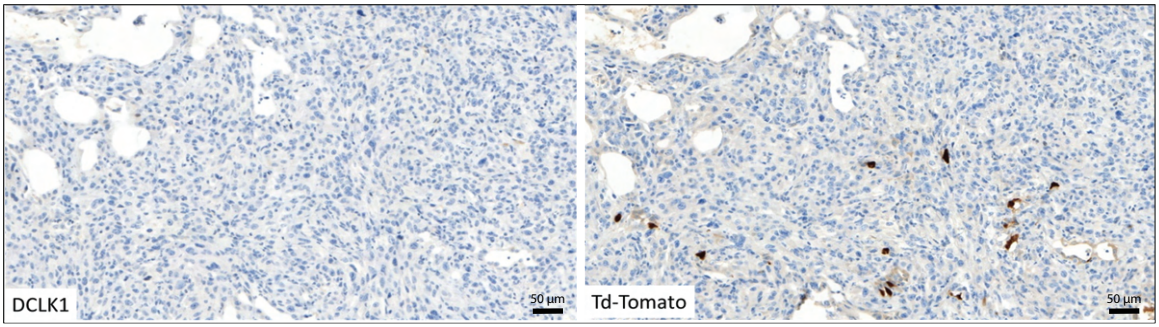

B **KPF-P2f3T**

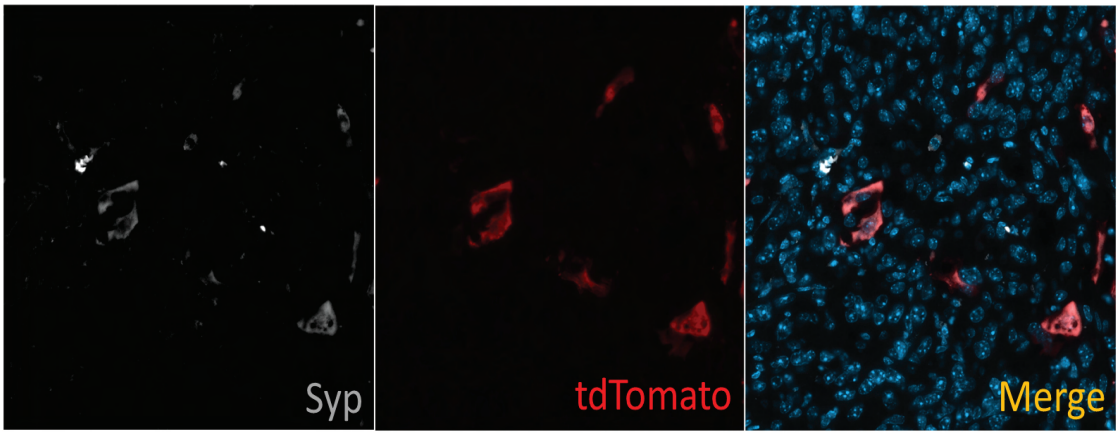

Figure 6

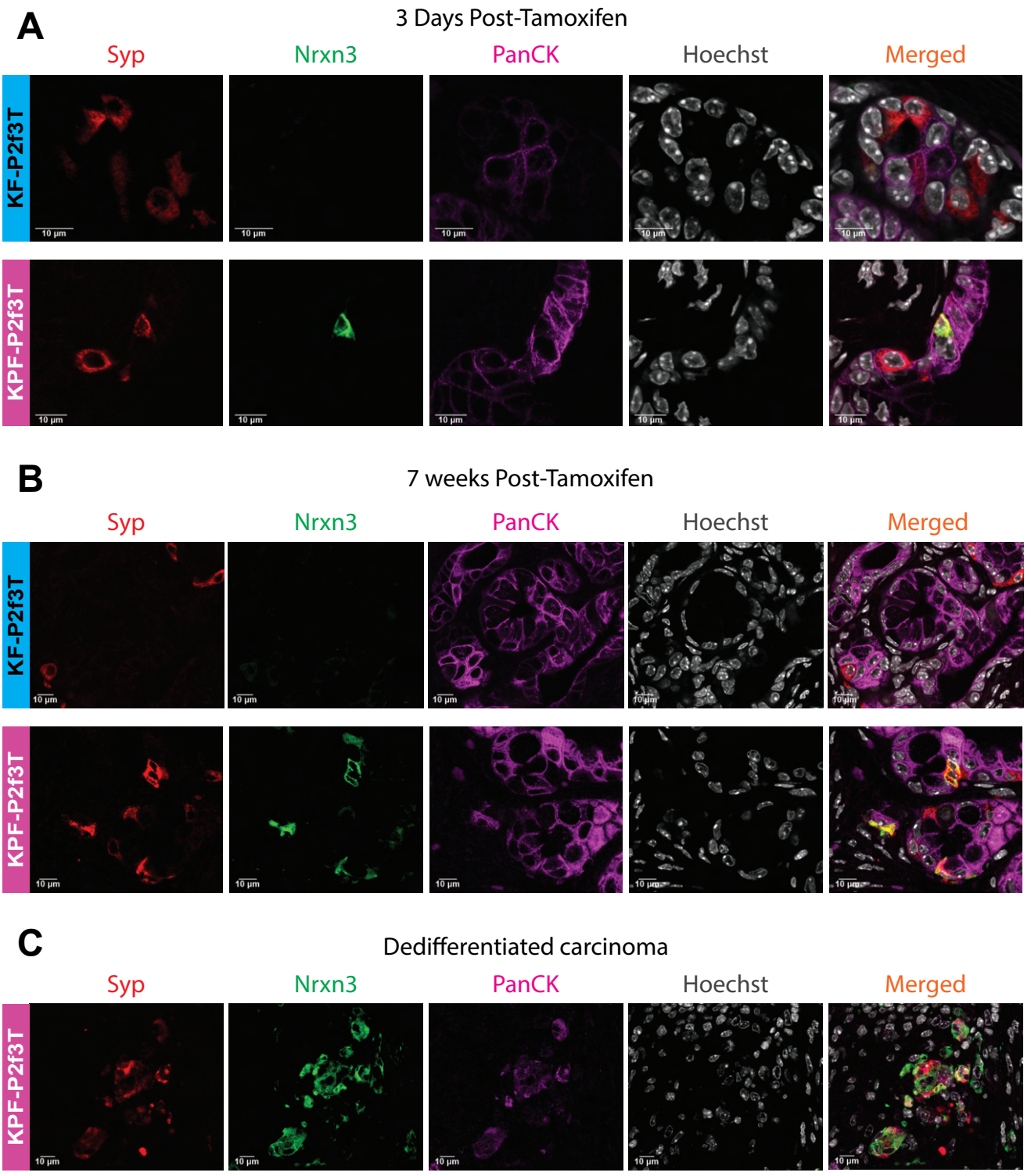
A
3 Days Post-Tamoxifen
Syp
Nrxn3
PanCK
Hoechst
Merged
KF-P2f3T
KPF-P2f3T
10 µm
B
7 weeks Post-Tamoxifen
Syp
Nrxn3
PanCK
Hoechst
Merged
KF-P2f3T
KPF-P2f3T
10 µm
C
Dedifferentiated carcinoma
Syp
Nrxn3
PanCK
Hoechst
Merged
KPF-P2f3T
10 µm

Figure 7

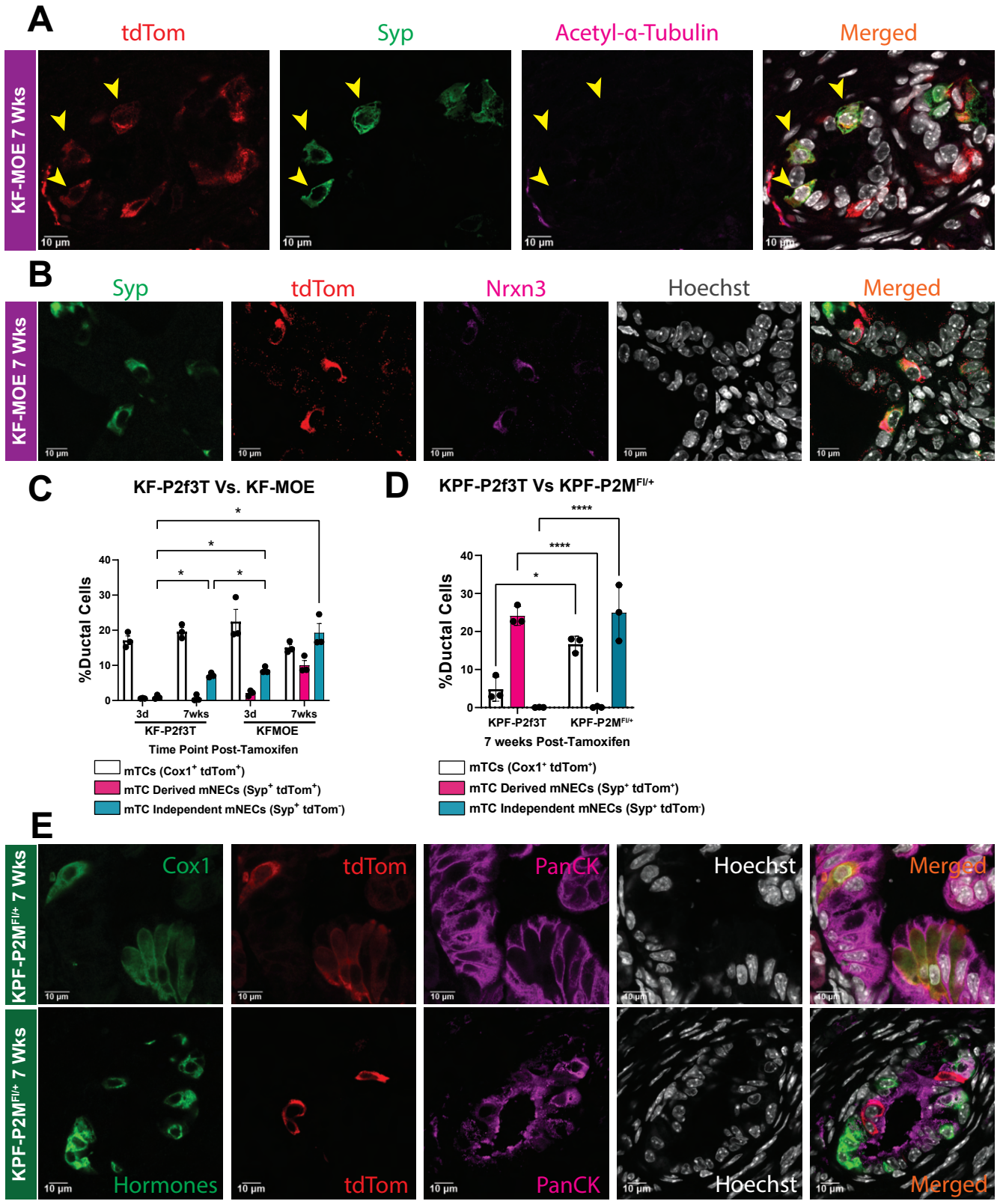
A
tdTom
Syp
Acetyl-α-Tubulin
Merged
KF-MOE 7 Wks
10 µm
B
Syp
tdTom
Nrxn3
Hoechst
Merged
KF-MOE 7 Wks
C
KF-P2f3T Vs. KF-MOE
%Ductal Cells
3d
7wks
KF-P2f3T
KFMOE
Time Point Post-Tamoxifen
mTCs (Cox1+ tdTom+)
mTC Derived mNECs (Syp+ tdTom+)
mTC Independent mNECs (Syp+ tdTom-)
D
KPF-P2f3T Vs KPF-P2M Fl/+
%Ductal Cells
KPF-P2f3T
KPF-P2M Fl/+
7 weeks Post-Tamoxifen
mTCs (Cox1+ tdTom+)
mTC Derived mNECs (Syp+ tdTom+)
mTC Independent mNECs (Syp+ tdTom-)
E
Cox1
tdTom
PanCK
Hoechst
Merged
KPF-P2M Fl/+ 7 Wks
Hormones
tdTom
PanCK
Hoechst
Merged
KPF-P2M Fl/+ 7 Wks